

RICH TOMOGRAPHY TECHNIQUES FOR THE ANALYSIS OF MICROSTRUCTURE AND DEFORMATION

Nikolaos Baimpas¹, Mengyin Xie¹, Xu Song², Felix Hofmann³, Brian Abbey⁴, James Marrow⁵, Mahmoud Mostafavi⁵, Jiawei Mi⁶ and Alexander M. Korsunsky^{1*}

¹Department of Engineering Science, University of Oxford,
Parks Road, Oxford OX1 3PJ, United Kingdom

² Singapore Institute of Manufacturing Technology, A*Star, 71 Nanyang Drive, Singapore, 638075

³ Chemistry Department, MIT, 77 Commonwealth Avenue, Cambridge, MA 02139-4307, USA

⁴ Melbourne University, School of Physics, Melbourne, Australia

⁵ Department of Materials, University of Oxford, Parks Road, UK

⁶ Department of Engineering, University of Hull, Hull, UK HU6 7RX

* e-mail: alexander.korsunsky@eng.ox.ac.uk, <http://www.eng.ox.ac.uk/elasticity>

ABSTRACT

Until very recently, the three-dimensionality of the material world presented numerous challenges in terms of characterisation, data handling, visualisation, and modelling. For this reason, 2D representation of sections, projections or surfaces remained the mainstay of most popular imaging techniques, such as optical and electron microscopy, and X-ray radiography. However, the advent of faster computers with greater memory capacity ensured that large 3D matrices can now not only be stored and manipulated efficiently, but also that advanced algorithms such as Algebraic Reconstruction Techniques (ART) can be used to interpret redundant datasets containing multiple projections or averages across the object obtained by some suitable analytical measurement technique. These tools open up unprecedented opportunities for numerical simulation. Model formulation can be accomplished semi-automatically on the basis of microstructurally-informed 3D imaging, while model validation can be achieved by direct comparison of 3D maps of complex quantities, such as displacement vectors or strain tensor components. In this paper we review several modalities of what can be referred to as “rich” tomography: strain tomography in the bulk of a load bearing structural component; Laue orientation tomography for non-destructive mapping of grain orientation within a polycrystal, and the use of sequences of tomographic reconstructions for Digital Volume Correlation (DVC) analysis of *in situ* deformation.

Key words: *rich tomography, Laue orientation tomography, strain tomography, Digital Volume Correlation*

1. INTRODUCTION

In recent years tomographic imaging has been established as a powerful tool for precise non-destructive evaluation of internal structure in materials. Driven by the industrial demand for high resolution 3D feature characterisation and quality inspection in engineering components [1, 2], recent research advances help to push the limits of imaging techniques [3, 4] to unprecedented levels of accuracy. Due to the complex geometries and miniaturization that are characteristic of modern engineering components, submicron spatial resolution is now

required, and more or less routinely achieved at dedicated state-of-the-art synchrotron radiation facility beamlines dedicated to X-ray Computerised Tomography (CT) [4-6].

In the present paper we make one further step in the development of these techniques, towards presenting the range of what we call “Rich tomography” techniques. This term we use to describe the suite of approaches that allow extracting additional three-dimensional information about the sample properties and state. “Rich tomography” serve to investigate non-destructively such complex quantities as internal strain distributions, grain shapes and lattice orientation, and even sub-grain crystal misorientations within bulk objects. While standard tomography is widely used for 3D imaging of density distributions, the new techniques that we describe below are referred to e.g. as “strain tomography” [7] and “Laue Orientation Tomography” [8]. Mathematically, these techniques can employ standard tomographic algorithms to reconstruct the complex tensor and vector quantities of interest, or can rely on more sophisticated algorithmic tools. In addition, preliminary strain analysis results are presented for *in situ* loading of composite materials, with their interpretation using the novel Digital Volume Correlation (DVC) technique. The range of potential applications of the method is discussed. The results demonstrate the power of the novel tomographic techniques, and pave the way to wider application of these approaches for better multidimensional characterisation of complex-shaped components under various loading conditions.

1.1 Experimental procedures for tomography & “rich tomography” data acquisition

The experimental basis of X-ray CT lies in the interaction of a penetrating X-ray beam with matter that results in the exponential attenuation of the beam with its passage through the material, according to the Beer-Lambert law. The logarithmic ratio of the transmitted versus incident intensity is linearly related to the integral of the absorption coefficient μ of the material along the path through the sample. The total mass absorption coefficient μ depends on the photoelectric absorption as well as the contributions from the coherent (Rayleigh) and incoherent (Compton) scattering. A convenient source of the numerical values for absorption coefficients of elements is, for example, the NIST database XCOM [9]. The X-ray image that is recorded on a CCD detector represents the projection of the sample volume under the incident X-ray illumination. After acquiring a large number of *projections* at equidistant angular positions between 0° and 180° , it is possible to *reconstruct* accurately the 3D density distribution function of the material using e.g. the standard filtered back-projection algorithms [10] or Algebraic Reconstruction Techniques (ART) [11].

Two principal experimental modes available to perform conventional (density) tomography are briefly described here. In the *absorption mode*, the difference in contrast, i.e. the ability to distinguish different materials and regions, mainly arises from the differences in the mass attenuation coefficient. The implementation of this technique is straightforward, and works better when objects contain regions with significant difference in atomic number and electron density [12]. A common problem is the generation of so-called imaging artefacts. These are features of the reconstructed images that do not correspond to the sample structure, but arise as the consequence of error magnification by the numerical reconstruction algorithm. The artefacts are related to beam hardening, beam focus, collimation, scintillators, sample drift, CCD pixel distortions etc. These aspects of the problem and ways of overcoming artefacts lie beyond the scope of this paper.

The *phase contrast mode* [13, 14] helps identify even small differences in the refractive index e.g. for materials with similar attenuation coefficients, where, especially at submicron resolution, the absorption mode fails to produce satisfactory reconstruction [14]. For phase contrast images to be obtained, the incoming beam should be at least partially coherent. Hence,

large source-sample distances are typically used at dedicated synchrotron imaging beamlines, while the sample-detector distances range from a few tens of centimetres up to a few metres, depending on the setup, the size of the sample and the refractive indices of the sample [15]. The presence of interfaces causes coherent beam to generate light-dark fringes that highlights these features. Increasing the sample - detector distance (propagation length) thus helps to emphasise the edges and interfaces of the object, and **also** allows one the detection of defects that are smaller than the pixel size, as shown by Cloetens et al. [16]. At larger distances, broad Fresnel fringes cover the image, turning it into a hologram with less and less direct resemblance to the object [17].

“Rich tomography” family of techniques that is the subject of the present report are employed to reconstruct different kinds of property distributions within the sample cross-section. These could be vector or tensor quantities (e.g. crystal orientation and strain, respectively), or possibly even more complex entities such as small angle scattering (SAXS) patterns. The reconstruction of strain distribution has been demonstrated by us using the procedure called *strain tomography* [7], while the relative lattice mis-orientation within individual grains was mapped using *Laue Orientation tomography* [8]. These are the two techniques developed in the present project and discussed below in the context of reconstructing the quantities with vector and tensor qualities that are more complex than scalars. With the help of “rich tomography”, additional information is extracted from the experimental data, while the non-destructive character of X-ray interaction with the sample is retained. The first encouraging results reported here pave the way for further developments of the methods that allow extracting more detailed information about the internal structure, as well as mapping strain, stress and crystal orientation in the bulk of engineering components.

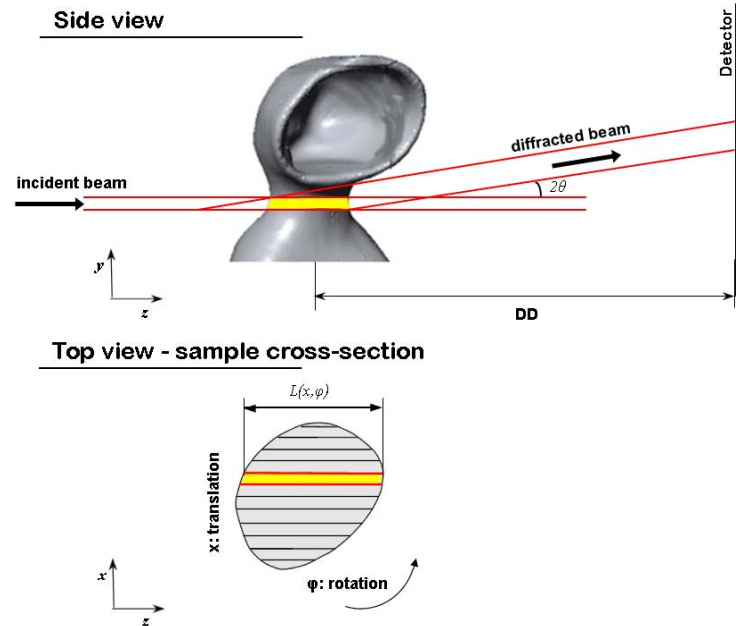


Fig 1. Example of strain tomography translate-rotate acquisition setup (a) side view (b) top view.

In absorption tomography, the logarithm of beam intensity p registered by each detector pixel is linearly dependent on the total absorption *integral* of the incident beam through the sample with the density distribution $\rho(x, y)$ within a particular cross-section. We note also that the 2D detector captures the data from each pixel simultaneously. In contrast, in strain tomography a small collimated beam is used that defines a single “pixel”. Measurements are made in a line scan over a set of points along the $-x$ -axis (perpendicular to the beam direction) that spans the

entire sample width. The sample is then rotated incrementally in small angular steps, so that the entire dataset for x and φ respectively is collected (Figure 1). For each beam position in x and φ , a diffraction pattern is obtained and is analysed by fitting single or multiple peaks. The strain value deduced from the interpretation of diffraction peak shift at each sample rotation and translation step (the translate-rotate technique) corresponds to the *average* value $q(x, \varphi)$ of the unknown strain along the path through the sample.

Although the difference between integral and average values is noted, in both cases the values that represent the experimental data depend *linearly* on the unknown quantity. Conversion from the average to the integral values is readily accomplished using the equation

$$p(x, \varphi) = \int_{L(x, \varphi)} q(x, y) dy = \langle q(x, \varphi) \rangle L(x, \varphi) \quad (1)$$

The above expression, sampled on a discrete grid of values of x and φ , represents the input for the filtered back-projection algorithm. The right hand side of (eq.1) is readily computed using element-wise product of the experimental data values and the matrix that contains the path length $L(x, \varphi)$ for each stage of the translate-rotate experiment. Thus, provided the sample shape is known, efficient inversion (reconstruction) is possible.

1.2 Digital volume correlation

Digital volume correlation (DVC) is a state-of-the-art technique that is capable of full field three-dimensional displacement evaluation. Its ability to extract 3D internal deformation is particularly useful in understanding the mechanical behaviour and capabilities of various engineering components [18, 19]. High-resolution X-ray microtomography data, acquired at consecutive loading increments during an *in situ* loading experiment, provide typical input for the analysis. Similarly to the 2D digital image correlation (DIC), the basic principle of DVC lies in the matching (or tracking) of features from the reference volume image to the deformed volume image, with best match determining the relative displacement vector. To obtain three-dimensional mapping of the displacement field, cubic sub-volumes surrounding each point in a grid located in the reference volume image are selected [20]. The corresponding locations in the deformed volume image are identified and a 3D grid of 3D displacement vectors is calculated. Although fundamentally simple in principle, the practical implementation of DVC involves significant challenges, including implementation complexity, measurement accuracy and computational efficiency. In the present report we discuss DVC interpretation of conventional absorption tomography datasets and the validation of Finite Element modelling by comparison with DVC analysis.

2. STRAIN TOMOGRAPHY

Contemporary synchrotron X-ray facilities provide high energy beams of superior penetrating ability and allow transmission imaging and scattering access to the interior (bulk) of materials and components. Materials diffract the X-rays strongly from sets of crystal lattice planes that provide an “atomic strain gauge” that allows the measurement of the average elastic strains within the scattering volume. By way of demonstration, the recently proposed technique of strain tomography [21] was first used to investigate the distribution of internal strain within a fixed prosthetic denture (FPD) made from polycrystalline zirconia. The FPD was subjected to a simulated mastication load [7]. A monochromatic X-ray beam was used to illuminate the sample, and a 2D detector was used to collect diffraction patterns, as illustrated schematically in Figure 1. The incident beam was monochromated to have the photon energy $\sim 90\text{keV}$, and collimated to the spot size of $0.1 \times 0.1\text{mm}^2$ on the sample. During data collection, the sample

was translated perpendicular to the beam, so that effectively the beam traversed the entire thickness of the sample in a step-wise fashion. At each position the beam was scattered to form a set of Debye-Scherrer rings. The translate-rotate technique mentioned previously was used to acquire a redundant set of diffraction patterns at a sufficient number of sample rotations (3.6° angular step) allowing the two-dimensional distribution of strain to be reconstructed, at the resolution corresponding to the transverse size of the beam.

2.1 Sample

An all-ceramic dental bridge framework made from anatomically reduced bridge copings using Wieland ZENO[®] Zr sintered zirconia ceramic material (Wieland Dental + Technik, Pforzheim, Germany). Wieland ZENO[®] Tec high temperature sintering process was used to manufacture the framework that was left uncoated (no porcelain veneer applied). The sample was mounted in a specially designed *in situ* three-point bend rig allowing to apply the simulated mastication force. The investigation was carried out on the synchrotron beamline ID15B (ESRF), using the setup shown in Figure 2. To aid the analysis, absorption tomography dataset was also collected at the HEX-lab X-ray tomography setup [3] in the Department of Engineering Science, University of Oxford. For the reconstruction of the 3D volume and image rendering (Fig. 2b) we used the filtered back-projection routines available in MATLAB[®]. The 3D solid model was converted to a Finite Element mesh using Simpleware[®] software. The resulting model is illustrated in Figure 2(c), together with the contour plot of the equivalent von Mises stress computed under the application of 300N nominal mastication load applied on the central unit, with the support provided by fixation of the two outer units on a simulated jaw base.

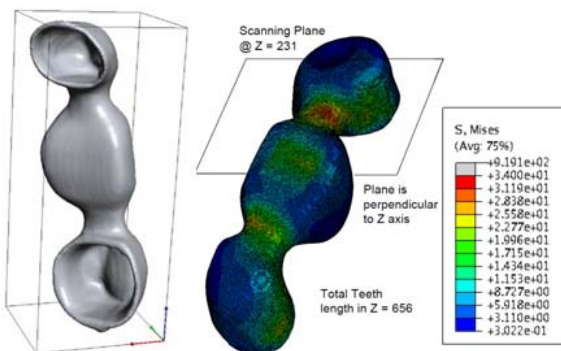
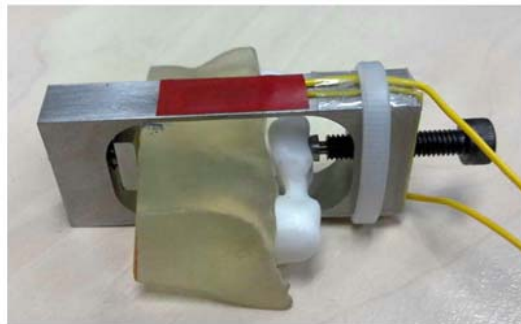


Figure 2. Fixed prosthetic denture (FPD) study: (a) three-point bending rig (PMMA support; load applied via pin) with load-cell (b) FPD shape from laboratory X-ray tomography. (c) FE model of the three-unit dental prosthesis under load of 300N.

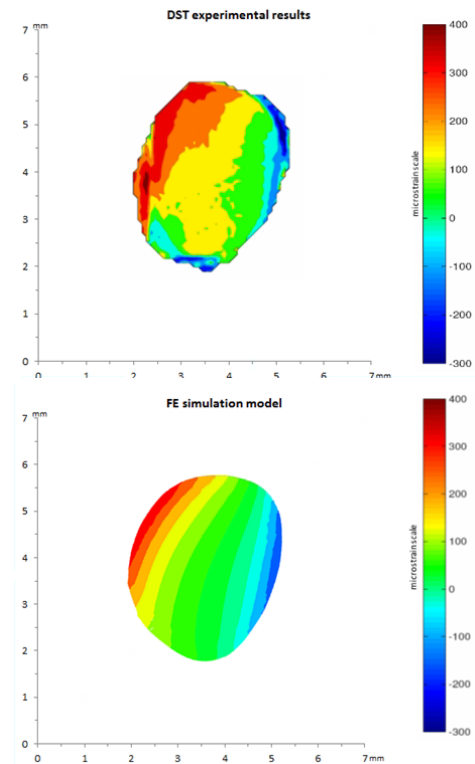


Figure 3. (a) Strain contour plot from tomographic reconstruction under 300N nominal applied load. (b) Corresponding FE model strain distribution.

2.2 Results

The interpretation of the diffraction patterns in terms of average strains and the inversion for the determination of internal strain distributions were accomplished using the procedures described in [7]. The resulting strain map reconstruction is shown in Figure 3(a) and compared with the Finite Element strain evaluation result in Figure 3(b) for the same cross-section under identical load. Direct comparison of the results shows the effectiveness of the technique proposed. While satisfactory agreement is observed, focusing on the detailed disagreements between the graphs is the next necessary step that can further guide the development of the technique.

3. LAUE ORIENTATION TOMOGRAPHY

In high performance engineering applications strain gradient related phenomena affect the mechanical response of materials. This is especially important where “weakest link” mechanisms such as fatigue, crack initiation and nucleation are triggered. An approach first introduced by Ashby [22] discriminates between *homogeneous plastic deformation*, accommodated by an arbitrary distribution of statistically stored dislocations (SSDs), and *inhomogeneous elastic-plastic response* of differently oriented neighbouring grains during deformation, accommodated by a distribution of geometrically necessary dislocations (GNDs). Building on that theory various approaches provided insight into the effects of microstructure on macroscopically observed phenomena [23, 24]. The validation of these theories requires suitably sensitive and spatially resolved probes that register the properties of crystal lattices (such as interplanar spacings) and distortions.

Micro-beam Laue diffraction is a well-established experimental technique that is capable of probing lattice spacing and structure, as well as the intra-granular lattice orientation of individual crystallites in the bulk of polycrystalline engineering alloys [25, 26]. When used in reflection mode the technique typically uses a polychromatic X-ray beam focused to a sub-micron spot and photon energies ranging usually from 2 to 25keV. Its unique ability to examine individual grains has been successfully used to map orientation, relative sub-grain misorientation [26], as well as elastic deformation [27]. The relatively soft energy spectrum used for micro-beam Laue setups limits the information available to surface and near surface regions ($\sim 70\mu\text{m}$). The recently proposed version of the method using harder X-rays ($>50\text{keV}$) [25] enabled transmission experimental setup to be used and for the integral through-thickness information to be collected.

3.1 Sample

A small bar about 10mm in length and approximately square cross-section was cut from 300 μm -thick Commercially Pure (CP) Ni sheet. Heat treatment under vacuum was carried out at 1200°C for 4 hours, followed by a furnace cool over 24 hours. This process ensured complete recrystallization and sufficient crystal growth so that individual grains were large enough to be imaged with sufficient spatial resolution using a 20 μm wide beam.

3.2 Results

The data analysis is described by Hofmann et al. [8]. Key aspects of the analysis procedure are:

- Ellipsoidal masks proposed by Gupta [26] are used to identify and “harvest” the Laue spot intensities for each grain

- A new routine is introduced that is able to eliminate (at least partially) some overlapping Laue spots produced by adjacent grains that contain annealing twins, thus producing overlapping patterns on the detector
- Simultaneous Algebraic Reconstruction Algorithm (S-ART) is implemented in MATLAB[®] and used for the reconstruction, and is shown to be superior in the case of limited spatial resolution and a small number rotation increments available

Five grains were identified in the illuminated volume. Reconstructions of each grain are given in Figure 4. Then the reconstructed intensity of all grains is added up and represented with the contour plot in the middle of Figure 4. The overlapping effect is still present making the outline of twinned grains (2-3) and (4-5) somewhat vague. Grains 2-3 showed a 109.5° relative rotation about $[011]$ axis, whereas grains 4-5 were found to have a 70.5° rotation around $[110]$ axis. Both these $\Sigma 3$ twinning relations are typical for fcc materials. These phenomena are described in some detail by M. Dechamps et al. [28].

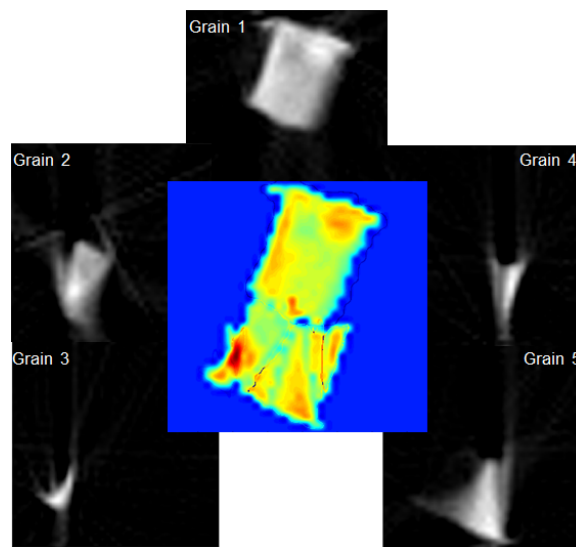


Figure 4. Reconstructions of grains 1 to 5 using S-ART (Algebraic Reconstruction Techniques). In the middle there is a contour plot of the entire cross-section reconstruction from summation of total intensity.

A colour representation of sub-grain mis-orientation is illustrated in Figure 5. Sub-grain misorientation for the specific sample was found to amount to less than 0.5° . We chose to use the incremental Rodriguez Vector (RV) representation that for small mis-orientations is additive, i.e. for three small mis-orientations RV12, RV23 and RV13 the following vector relation holds: $RV13 = RV12 + RV23$. This allows us to treat each component of the Rodriguez vector as a separate quantity and reconstruct the three RV components (RV_1 , RV_2 , RV_3). A unique colour from the RGB colour scale was then assigned to each of the reconstructed vector components (RV_1 -Red, RV_2 -Green, RV_3 -Blue). The values on each one were normalised with respect to the biggest $(RV_{1,2,3})_{\max}$ value of all three components. Using this convention, the effect of misorientation of each component is reflected in the intensity contribution from each of the RGB colour components. The components are all shown together in the sketch at the bottom of Figure 5 using 8-bit RGB representation. So far this appears to offer the best way to depict the contribution to misorientation from different RV components on a single diagram. Better resolution (i.e. smaller beam size) would increase the total number of pixels in the reconstruction, giving a more precise determination of the orientation distribution.

A natural choice of laboratory-based method for comparison of our reconstruction results is electron back-scattered diffraction (EBSD) that is performed within the SEM. In comparison with X-ray micro-beam Laue diffraction, EBSD currently provides superior spatial resolution

down to a few nm, but typically has lower angular resolution, due to the electron beam divergence as a consequence of electromagnetic lens focusing. This can be improved, however, by replacing direct determination of lattice orientation with comparative pattern rotation analysis using Digital Image Correlation [29].

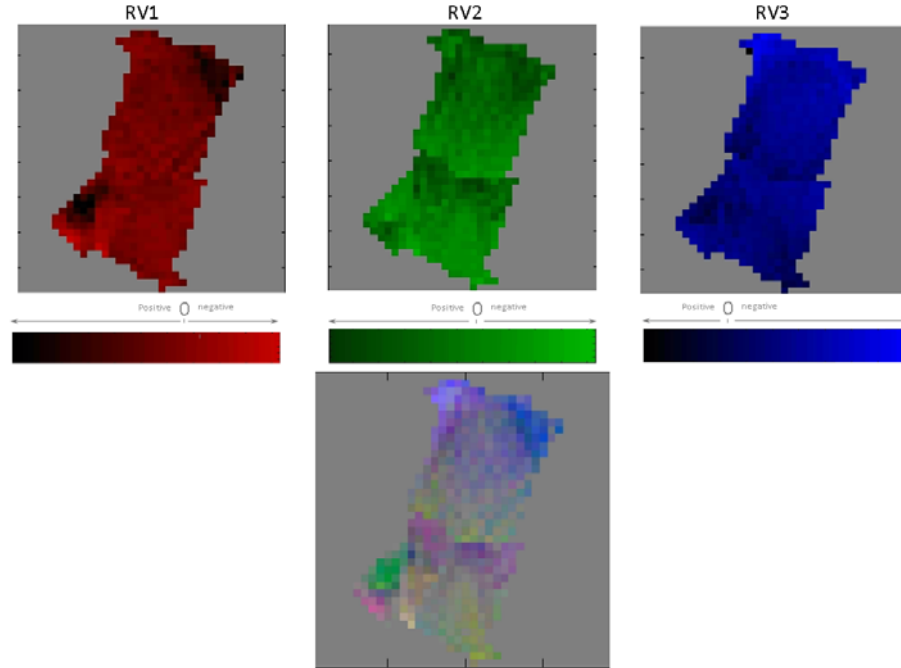


Figure 5. Top row: RGB colour assignment for each component of the Rodriguez vector. Bottom: RV space misorientation representation obtained by adding up individual components. Shades that are lighter or darker than the grey background represent larger rotation angles.

4. DIGITAL VOLUME CORRELATION

The mechanical behaviour of ductile metal-metal composites is an area of study that has direct relevance to a range of industrial and research applications. The behaviour of these materials differs from conventional matrix composites in that both matrix and reinforcing phase are ductile metals [30]. Typically, metal-metal composites are manufactured using co-spray forming methods [31], and may involve blending together a face centred cubic (fcc) metal with a body centred cubic (bcc) metal, e.g. Cu–Nb or Al–Nb, or an fcc metal with a hexagonal close-packed (hcp) metal, e.g. Al–Ti. In the present study an Al–12Si alloy + 12% Ti specimen was studied by absorption tomography under multi-stage *in situ* compression. A small rectangular sample with the approximate size of 1 mm(*l*) \times 1 mm(*w*) \times 1.5 mm(*h*) was cut out from a 1mm \times 20 mm extruded strip. In the co-spray manufacturing process, Ti powder was mixed with Al–Si alloy droplets primarily during atomisation of the Al–Si melt stream and co-deposited into a billet. Additional extrusion to a true strain of ~ 6.1 was also conducted to enhance the materials properties [32]. An experimental study was carried out to collect microstructural information during multiple increments of loading, and to extract quantitative information about the mechanical response, by combining high resolution micro-tomography and Digital Volume Correlation (DVC).

4.1 Setup - Analysis

Tomography

A hard X-ray micro-tomography setup available at the TOMCAT beamline in Swiss Light Source (SLS) was used. The beam was monochromated to 20keV, a 20 micron thick scintillator (type: YAG:Ce) was used as a trade-off of speed versus resolution along with an objective (UPLAPO10x) offering a $1.5 \times 1.5 \text{ mm}$ field of view and $0.74 \times 0.74 \mu\text{m}$ pixel size. Exposure time was adjusted to 700ms for optimum contrast result. 1200 projections were collected at an angular step of 0.15° from 0° to 180° . The sample was mounted within a custom made loading rig and tomography data sets were collected at 10 deformation increments. The current rig does not allow measurement of the sample load. The total nominal strain applied was about 2.6%. As will be seen below, however, local regions within the sample experienced lower or higher strain levels due to sample slipping and bending.

Digital Volume Correlation (DVC)

DVC operates by evaluation cross-correlation of paired datasets. Two strategies can therefore be adopted to analyse the deformation of the specimen: either the dataset from each loading stage is correlated against the first reference dataset, or each dataset may correlated against its preceding loading stage. As the specimen experienced significant deformation at each loading stage in this experiment, the incremental approach was employed.

As explained previously, DVC is performed on patches of voxels, often referred to as “windows”. Each patch in the reference state is correlated with its counterpart after loading, and its relative displacement is calculated. Correlation is an iterative process; a large window size is first selected and its average displacement is calculated; then it is broken down into smaller sub-windows, and the average displacement of each sub-window is calculated. This process may be continued until the sub-window does not contain enough features for the correlation function to achieve a match. Larger windows achieve higher precision, of up to a few % of a voxel; the uncertainty in the displacement vector determination increases exponentially with decreasing window size. Window overlapping may be employed, increasing the number of calculated displacement vectors. This is helpful when the displacement gradients are sufficiently shallow, but may not provide useful information about deformation that is more heterogeneous, e.g. at the length-scale of the microstructure.

StrainMaster Davis 8.0 [32] digital volume correlation software was used in this study. The dataset comprised $1789 \times 1609 \times 2048$ voxels. A initial window of $512 \times 512 \times 512$ was used, followed by windows of $256 \times 256 \times 256$, $128 \times 128 \times 128$ and then $64 \times 64 \times 64$ voxels; 50% overlap was used at all levels.

Finite element modelling

The loads applied to the sample were not recorded in this experiment. However, a finite element model can be constructed by applying displacement boundary conditions obtained from DVC analysis of the top and bottom boundaries of the sample. This allows comparison to be made between DVC and FE. The Ramberg-Osgood material model was used to describe the material properties of the Aluminium – Titanium composite. We note that the original state of the specimen was not available, i.e. the initial observation of on the specimen was made when it already had experienced plastic deformation (loading stage 1). Hence, the yield stress in the FE model was defined at a very low value (1 MPa). This essentially caused the model to show plastic deformation from the first stage of deformation. The elastic modulus and Poisson’s ratio were set at 67 GPa and 0.33, typical of most aluminium alloys. The hardening exponent was varied. The specimen was meshed in a way that a node existed at the same locations as the

displacement vectors calculated from DVC. Overall, 58800 20-node brick elements were used. The distribution of plastic strains could be predicted by varying systematically one model parameter, namely, the exponent parameter n . The results of the simulation were compared with DVC displacements fields, and the value of the adjustable parameter was sought that provided the best match between the FE prediction and DVC evaluation.

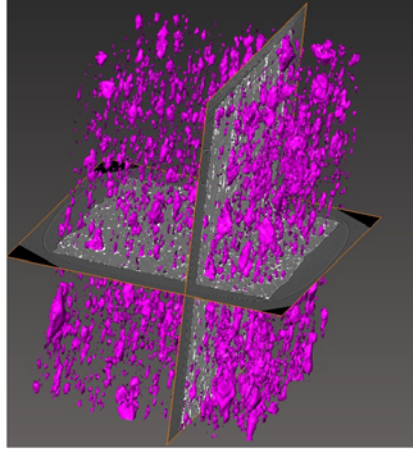


Figure 6. 3D image rendering of the Ti reinforcement phase.

4.2 Results

Examples of central vertical slices through the tomographic reconstruction of the sample at consecutive loading increments $N=1$ to 10 are shown in Figure 7. The Ti reinforcement phase exists in the form of thin fibrous inclusions along the extrusion direction, as well as some more equi-axed “bulbs”. These results show excellent agreement with SEM microscopy results of Kelly et al [30]. The complex sample response to loading is manifested in the appearance of bending from $N=5$ and continues to develop further until the last loading increment ($N=10$). Additionally, some rigid body displacement of the specimen (drift) across the field of view at higher loading increments is also observed.

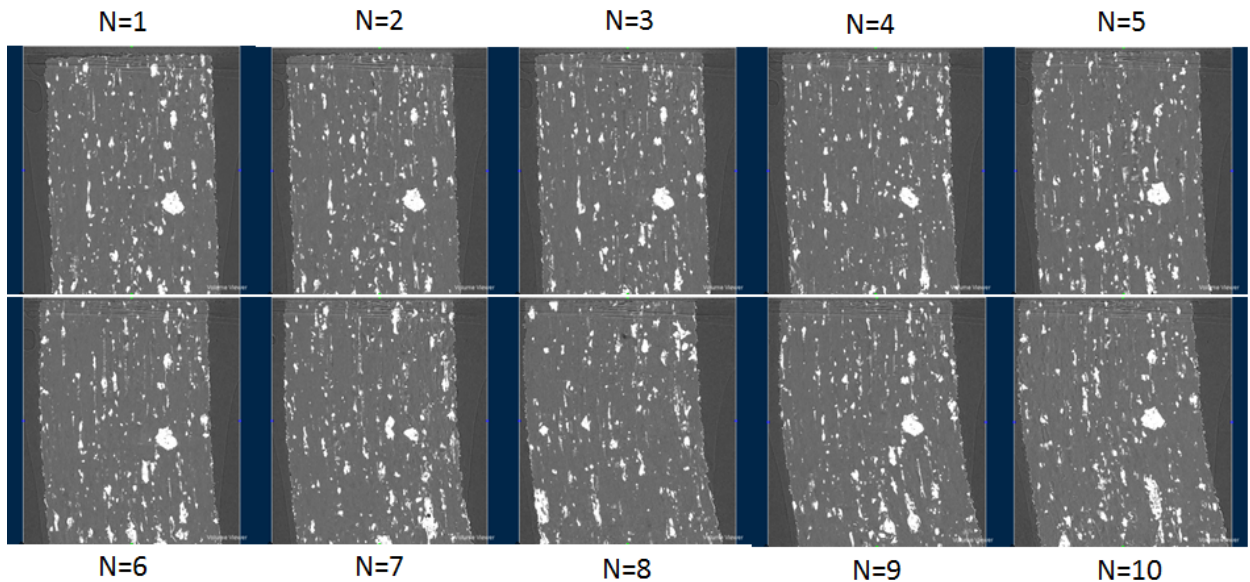


Figure 7. Tomographic reconstruction of the central vertical cross-section for consecutive loading increments: $N=1$ to 10.

The tomography data (Figure 7) show clearly that the specimen experiences combined bending and compression during loading. Overall, deformation is not uniform within the sample. The same trend is also seen clearly in the DVC results (Figure 8), where examples of the measured displacement fields are shown for the same vertical slice. The rigid body movements, due to sample rotation and drift, were removed by DVC analysis.

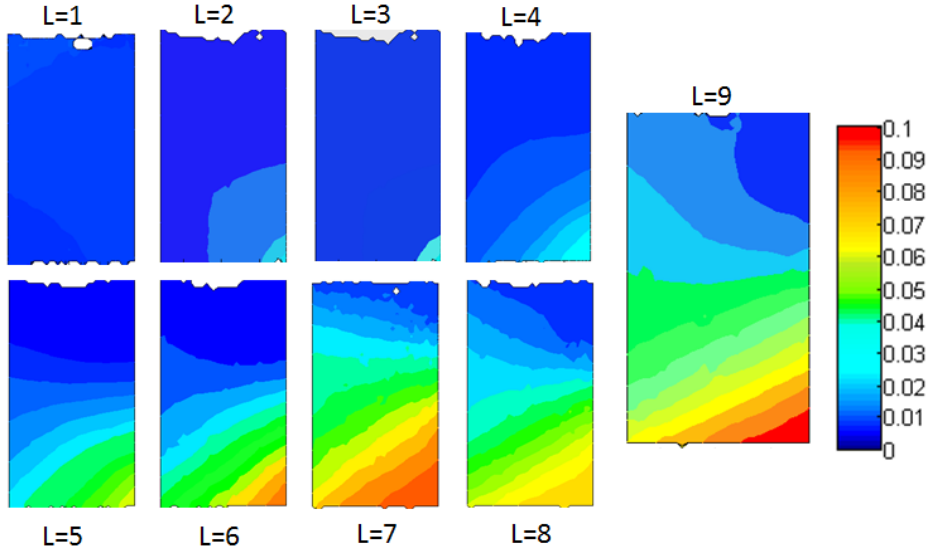


Figure 8: Consecutive loading stage displacement field obtained from DVC (sample width = 1 mm).

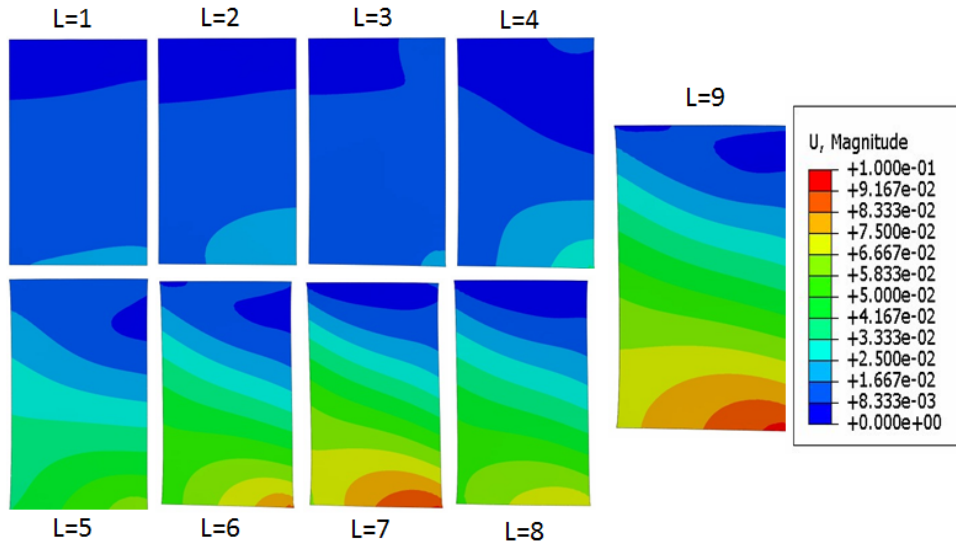


Figure 9: Consecutive loading stages from ABAQUS FE model (sample width = 1 mm).

Similar results were obtained from the finite element simulation. Figure 9 shows the displacements calculated from the FE model for the same slices as shown in figure 8. The agreement between DVC and FEM data was best when the exponent parameter of 9 was used. We note, however, that for the present case this value is not necessarily representative of the material strain hardening exponent. This is due to the limitations of the loading rig used, and the tomographic datasets collected starting from an already deformed sample. A much more accurate measure can be readily obtained by using accurate load cell readings and displacement data obtained by DVC analysis of deformation.

The type of analysis of 3D deformation presented above, combined with accurate measurement of applied loads, can offer excellent facility for extracting unknown mechanical properties (stiffness, Poisson's ratio, flow behaviour) from observing the bulk response of materials that undergo complex deformation, and is likely to be particularly useful for small specimen testing. By way of comparison, Figure 10 shows the range of maximum principal strains within the specimen as a function of the loading stage. The excellent agreement between DVC and FEM in terms of the overall trend and the spread of strain values in the sample is evident.

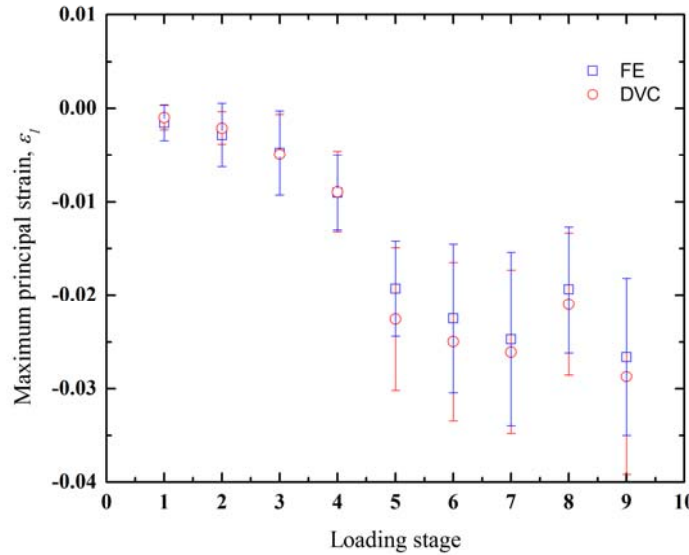


Figure 10: The ranges of maximum principal strains across the entire sample at each loading stage calculated by DVC and compared to FE modelling results.

5. CONCLUSIONS

This report presented a selection of advanced tomographic techniques and interpretation procedures that provide a perspective on the likely future development directions in the field. The advancement of tomographic reconstruction modalities and algorithms is necessitated by the growing scientific and engineering need to interrogate real three-dimensional objects in a non-destructive way, yet so as to access a variety of important physical and mechanical parameters, such as crystal orientation and quality, lattice distortion and mis-orientation, elastic and plastic components of the strain tensor, etc.

Advancement towards these goals is likely to involve X-ray techniques, as these beams of (high energy) photons provide a unique non-destructive probe that is sensitive to all aspects of material's electronic, crystallographic and micro-structure. On the one hand, we expect further progress to be made towards improving the spatial resolution beyond the current record of $\sim 7\text{nm}$ beam spot size [33]. On the other hand, we expect the development of both experimental techniques and algorithms for measuring and reconstructing ever more intricate and complex quantities that describe material behaviour, both mechanical and functional. The data obtained in this way lends itself naturally to direct validation of modern 3D simulations of deformation and other related parameters, e.g. fracture, voiding, polarization, etc.

Another interesting avenue of development for these techniques concerns their application for *elastography*. This is a term used to refer to the determination of the (elastic) properties of an object (and its constituents) by matching numerical simulation results to observations. This type

of inverse problem can be readily tackled in the spirit of DVC-FEM matching described here. This seems particularly relevant in the medical context, such as e.g. breast cancer screening.

REFERENCES

1. Moller-Gunderson D, When 2D X-ray isn't enough. SMT, 2007: 8.
2. Obrist A, First Article Inspection Based on Industrial X-ray Computed Tomography Materials Testing and Research International Conference, 2001. Nuremburg: p. 177-180.
3. Korsunsky AM, Xie M, Baimpas N, Song X, X-ray Texture Analysis and Imaging of Engineering Materials at Oxford HEX-lab, in Proceedings of the International MultiConference of Engineers and Computer Scientists 2012. 2012, IMECS 2012: Hong Kong.
4. Stampanoni MG, Isenegger A, Mikuljan G, Chen Q, Bertrand A, Henein S, Betemps R, Frommherz U, Böhler P, Trends in synchrotron-based tomographic imaging: the SLS experience. Proceedings of SPIE, 2006. 6318:63180M--63180M-14.
5. ESRF. Coherent Image Formation, Absorption and Phase-Contrast Tomography, <http://www.esrf.eu/UsersAndScience/Experiments/Imaging/ID22/Applications/Imaging/CoherentImage>. 2011.
6. Beckmann F, Lippmann T, Lottermoser L, Martins RV, Schreyer A, The new materials science beamline HARWI II at DESY. Proceedings of SRI 06. AIP Volume 879: p. 746-749
7. Korsunsky AM, et al., Strain tomography of polycrystalline zirconia dental prostheses by synchrotron X-ray diffraction. Acta Materialia. 2011; 59:2501-2513.
8. Hofmann F, Connor L, Baimpas N, Song X, Keegan S, Korsunsky AM, Imaging of grain-level orientation and strain in thicker metallic polycrystals by high energy transmission micro-beam Laue (HETL) diffraction techniques. International Journal of Materials Research. 2012, 103:8.
9. Berger MJ, Hubbell JH, Seltzer SM, Coursey JS, Zucker DS, XCOM: Photon Cross Section Database 1.2, available online at <http://physics.nist.gov/xcom>. 1999.
10. Herman GT, *Image Reconstruction from Projections*. Academic Press, 1980. **New York**(1980).
11. Kak AC and Slaney M, *Principles of computerized tomographic imaging*. Engineering in Medicine. 1988, Biology Society: IEEE Press.
12. Salvo L et al., X-ray micro-tomography an attractive characterisation technique in materials science. Nuclear Instruments and Methods in Physics Research Section B: Beam Interactions with Materials and Atoms, 2003. **200**(0): p. 273-286.
13. Donath T, Pfeiffer F, Bunk O, Groot W, Bednarzik M, Grünzweig C, Hempel E et al., Phase-contrast imaging and tomography at 60 keV using a conventional x-ray tube source. Review of Scientific Instruments, 2009. **80**(5), **053701**.
14. Stampanoni M et al., Phase-contrast tomography at the nanoscale using hard X-rays. Physical Review B, 2010. **81**(14): p. 140105.
15. Snigirev A, Snigireva I, Kohn V, Kuznetsov S, Schelokov I, On the possibilities of X-ray phase contrast microimaging by coherent high-energy synchrotron radiation. Rev. Sci. Instr., 1995. **66**: p. 5486-5492.
16. Cloetens P, Buffiere JY, Peix G, Baruchel J, Peyrin F, Schlenker M, Observation of microstructure and damage in materials by phase sensitive radiography and tomography, J. Appl. Phys., 1997. **81**(9).
17. Cloetens P, *Phase Contrast Imaging -Coherent Beams*. 2007: School on X-ray imaging Techniques ESRF.

18. Bay B et al., Digital Volume Correlation: Three-dimensional strain mapping using X-ray tomography. *Experimental Mechanics*, 1999. **39**(3): p. 217-226.
19. Forsberg F, Siviour CR, 3D deformation and strain analysis in compacted sugar using x-ray microtomography and digital volume correlation. *Measurement Science and Technology*, 2009. **20**(9): p. 095703.
20. Pan B, Wu D, Wang Z, Internal displacement and strain measurement using digital volume correlation: a least-squares framework. *Measurement Science and Technology*, 2012. **23**(4): p. 045002.
21. Korsunsky A.M., et al., The principle of strain reconstruction tomography: Determination of quench strain distribution from diffraction measurements. *Acta Materialia*, 2006. **54**(8): p. 2101-2108.
22. Ashby MF, The deformation of plastically non-homogeneous materials. *Philosophical Magazine*, 1970. **21**(170): p. 399-424.
23. Gaucherin G et al., Crystal plasticity and hardening: A dislocation dynamics study. *Procedia Engineering*, 2009. **1**(1): p. 241-244.
24. Meissonnier FT, Busso EP, O'Dowd NP, Finite element implementation of a generalised non-local rate-dependent crystallographic formulation for finite strains. *International Journal of Plasticity*, 2001. **17**(4): p. 601-640.
25. Hofmann F et al., High energy transmission micro-beam Laue synchrotron X-ray diffraction. *Materials Letters*, 2010. **64**(11): p. 1302-1305.
26. Gupta VK, Agnew SR, Indexation and misorientation analysis of low-quality Laue diffraction patterns. *Journal of Applied Crystallography*, 2009. **42**(1): p. 116-124.
27. Hofmann F, *Probing the Deformation of Ductile Polycrystals by Synchrotron X-ray Micro-diffraction*, D Phil thesis, Department of Engineering Science, University of Oxford (2011).
28. Déchamps M, Baribier F, Marrouche A, Grain-boundaries: Criteria of specialness and deviation from CSL misorientation. *Acta Metallurgica*, 1987. **35**(1): p. 101-107.
29. Britton TB, Wilkinson AJ, High resolution electron backscatter diffraction measurements of elastic strain variations in the presence of larger lattice rotations, *Ultramicroscopy*, 2012, **114**.
30. Russell AM, Chumbley LS, Tian Y, Deformation Processed Metal–Metal Composites. *Advanced Engineering Materials*, 2000. **2**(1-2): p. 11-22.
31. Kelly AJ, et al., An Al–Si–Ti hierarchical metal–metal composite manufactured by co-spray forming. *Journal of Materials Processing Technology*, 2011. **211**(12): p. 2045-2049.
32. DaVis, *User's Manual*. 2009, Gottingen: LaVision GmbH.
33. Mimura H, Handa S, Kimura T et al., *Nat. Phys.* 6 (2010) 122.